Astrostationary orbits for hybrid space and ground-based observatories

Eliad Peretz[a,*] **Christine Hamilton**[a] **John C. Mather**[a] **Simone D'Amico**[b] **Adam Michaels**[a] **Robert Pritchett**[a] **Wayne Yu**[a] **and Peter Wizinowich**[c]

[a]NASA Goddard Space Flight Center, Greenbelt, Maryland, United States
[b]Stanford University, Space Rendezvous Laboratory, Palo Alto, California, United States
[c]W. M. Keck Observatory, Mauna Kea, Hawaii, United States

Abstract. Ground-based observatories' capabilities can be greatly enhanced by working with satellites in astrostationary orbits. Satellites inertially aligned with ground-based observatories can help mitigate atmospheric effects in astronomical, solar, and planetary observations. We present a method for developing and modeling the trajectory of potential astrostationary orbits as seen from the ground to understand whether they meet defined astrostationary conditions such as the location in the field of interest and the observation time. It discovers an L2 orbit family and shows that it can meet astrostationary conditions. It then presents an example mission, Orbiting Configurable Artificial Star (ORCAS), in which a satellite aligns with a ground-based observatory to provide near-diffraction limited observations in the visible wavelength. A highly elliptical orbit family which can meet the ORCAS requirements is studied, and we go on to show how multiple observations can be made during a single-orbit period and how specific configurations that increase the observation time can be found. Finally, other potential astrostationary families are presented, as well as additional applications that could benefit from spacecraft and ground-based observatories working together, and future work which can be done to move forward in the field is discussed. © *2022 Society of Photo-Optical Instrumentation Engineers (SPIE)* [DOI: 10.1117/1.JATIS.8.1.014004]

Keywords: astrostationary; orbits; ground observatory; spacecraft.

Paper 21085 received Aug. 6, 2021; accepted for publication Jan. 4, 2022; published online Jan. 31, 2022.

1 Introduction

A ground-based observatory working in conjunction with spacecraft can enhance the capabilities of current telescopes while also removing some of the limitations inherent in ground and space telescopes. Although space observatories enjoy a lack of atmosphere, they suffer from higher costs, strict size constraints, and more risk. On the other hand, ground-based observatories can be much larger at a fraction of the cost and enable real-time hardware updates, but they are limited to working in Earth's atmosphere on the ground. Hybrid space and ground observatories offer the benefits of building on the ground while also offering the flexibility of space to aid in negating atmospheric effects, among other benefits. These hybrid systems would enable ground and space elements to perform synergetically to make both of them stronger.

There are several examples of mission concepts that aim to extend the capabilities of both ground and space observatories by using elements in each. One is adding a space-based component to the Event Horizon Telescope.[1] This could enable high time-resolution imaging (movies) of the supermassive black hole at the galactic center and other improvements to black hole science. In a second concept for a hybrid ground and space observatory, a starshade would be in a highly elliptical orbit (HEO) and would work with an observatory to block a target star, enabling the ground observatory to image exoplanets around the star.[2,3] Next, the Orbiting Configurable Artificial Star (ORCAS) mission would enable ground-based observatories, which

*Address all correspondence to Eliad Peretz, eliad.peretz@nasa.gov

2329-4124/2022/$28.00 © 2022 SPIE

Downloaded From: https://www.spiedigitallibrary.org/journals/Journal-of-Astronomical-Telescopes,-Instruments,-and-Systems on 24 Jul 2023
Terms of Use: https://www.spiedigitallibrary.org/terms-of-use

are currently limited by atmospheric distortion, to take images with unprecedented angular resolution and sensitivity. ORCAS would provide a laser guide star in the field of interest (FOI) of a ground telescope and the ground observatory would then be able to use adaptive optics (AO) to remove atmospheric distortion.[4–9] The ORCAS concept could also be applied to heliophysics using a spacecraft acting as a laser guide star to image the solar corona. This would enable at least one order of magnitude of improvement in the angular resolution of images of the corona.[10] These examples are only some of the potential applications of hybrid ground- and space-based observatories.

There is currently relatively little work on astrostationary orbits. In the past, most work has focused on using a laser guide star mounted on a satellite to reduce atmospheric distortion in astronomical images taken from the ground.[11–19] These works predominantly focus on using HEOs as an astrostationary orbit, with observations occurring at apogee. This work has been expanded on in the design of the ORCAS mission, which also proposes using a satellite with a laser payload flying in an HEO.[4] In addition to work on laser guide stars, work has also been done on a proposed mission which would fly a remote occulter in an HEO which would similarly align near apogee.[2] This type of mission has also been proposed for improving flux calibration.[20] However, ground observatories and spacecraft working together, especially in orbits that are not highly elliptical, are a relatively unexplored field.

This paper provides three contributions to the field. First, a method of modeling and simulation that would enable users to build an astrostationary orbit specific to their mission requirements and science goals is developed. This method provides the orbit trajectory, the spacecraft's path from the view of the ground station, plots of the drift rate across the orbit, among other results. This method will allow users to check whether any orbit could be used as astrostationary. Past work on astrostationary orbits has all focused on using HEOs, but in reality many different orbit families could be used. Therefore, the second contribution is identifying two orbit families which can be used as astrostationary orbits. The development of these orbits and results which show how they meet astrostationary requirements are presented. Finally, the third contribution is in the design and evaluation of an orbit for the ORCAS mission and demonstrating how an astrostationary orbit can be tuned to get better results. An HEO orbit is presented which has a novel three observation opportunities per orbit.

This paper starts out by describing the methodology used to develop the modeling and simulation for astrostationary orbits in Sec. 2. Two example astrostationary orbit families are developed which could be used in a variety of applications and results are presented showing how they meet astrostationary conditions in Sec. 3. In addition to the general foundation for astrostationary orbits, this paper also focuses on one example application, ORCAS. Section 4 develops and selects an orbit which meets the ORCAS mission requirements and presents further results on that orbit, including the possibility of making three observations in a single elliptical orbit and a method of tuning orbits to increase observation time. Finally, this paper concludes with a discussion of the results and other potential astrostationary orbits in Sec. 4 and conclusions in Sec. 5.

2 Methodology

There are several applications where ground observatories could work with space components to get unique results neither could achieve alone. These applications will all have different requirements and goals, so this paper focuses on specific applications which use astrostationary orbits to achieve their desired results.

An astrostationary orbit is defined as one where a space component in orbit aligns with a ground station and an astronomical object such as the Sun, a galaxy, a star, or another planet to achieve some goal. A model has been developed which can propagate an orbit and show it from different veiwpoints, including in the Earth centered inertial (ECI) frame, the view from the ground station, and the spacecraft's right ascension (RA) and declination (DEC) in the observable sky. In this section, this method is described in greater detail. The model used to generate orbits is presented along with the assumptions built into it. An astrostationary reference frame is then defined which can be used to generate results which allow for the comparison of astrostationary orbits.

Downloaded From: https://www.spiedigitallibrary.org/journals/Journal-of-Astronomical-Telescopes,-Instruments,-and-Systems on 24 Jul 2023
Terms of Use: https://www.spiedigitallibrary.org/terms-of-use

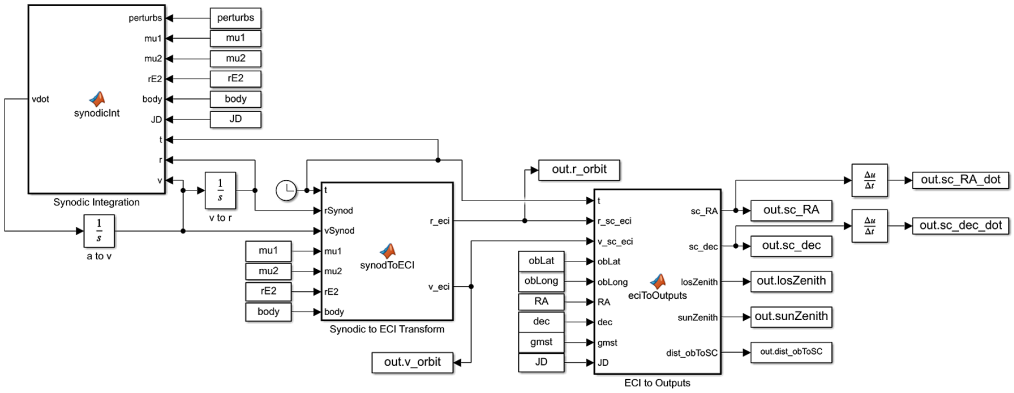

Fig. 1 Simulink model used to propagate orbits. Block on far left propagates the orbit in the synodic frame, middle block converts synodic position and velocity to ECI position and velocity, and right block converts ECI position and velocity to output values including the spacecraft RA and declination and key angles for the observatory.

2.1 *Model*

In this section, the method developed to model astrostationary orbits for hybrid ground-space observatories is described. Figure 1 shows the Simulink model used to propagate the orbits. As shown, the orbits are propagated in the synodic frame using numerical integration.[21,22] The synodic frame is used for integration because it can seamlessly support orbits in the restricted two- and three-body problems. The synodic frame is defined using the circular restricted three body problem. In this definition, two bodies, e.g., the Sun and Earth, are chosen, and two major assumptions are made: first, that those are the only two bodies with mass in the system, and second, that the bodies move in a circular orbit around the system barycenter. The $\mathbf{x}$ vector points from the barycenter to the smaller body at all times, rotating with the system, the $\mathbf{z}$ vector points in the direction of the system angular momentum, and the $\mathbf{y}$ vector completes the triad. The third body in this system is the spacecraft, which is treated as massless. The system can be modeled as an Earth/no body system for the two-body problem.

The Simulink model propagates the orbit in the synodic frame, converts the position and velocity to the ECI frame, and then converts those values to the spacecraft RA and declination and key angles for the observatory. To do this, it takes in the gravitational parameters for the larger and smaller body (μ_1 and μ_2, respectively), the distance between the Earth and the second body (r_{E2}), and a constant representing the second body (e.g., Sun or Moon). Additionally, the Julian date is fed to the system as well as the initial position and velocity of the orbit in the synodic frame. Finally, perturbations can be added to the model, including Earth's J2, Sun, and Moon perturbations. Once all the values have been selected, the equations of motion in the synodic frame used for this model are given by

$$\dot{\mathbf{v}}_{\text{syn}}^{\text{sc}} = -\frac{\mu_E \mathbf{r}_{\text{syn}}^{\text{sc}}}{\|\mathbf{r}_{\text{syn}}^{\text{sc}}\|^3} - 2\left(\begin{bmatrix}0\\0\\\omega_s\end{bmatrix} \times \mathbf{v}_{\text{syn}}^{\text{sc}}\right) - \begin{bmatrix}0\\0\\\omega_s\end{bmatrix} \times \left(\begin{bmatrix}0\\0\\\omega_s\end{bmatrix} \times \mathbf{r}_{\text{syn}}^{\text{sc}}\right), \tag{1}$$

where ω_s is the angular rotation of the synodic frame, the superscript sc indicates the value is for the spacecraft, and the subscript syn indicates the vector is in the synodic frame. The synodic position and velocity are then converted into the ECI frame using the same inputs as for the first (leftmost in Fig. 1) block. Finally, those vectors are converted into several useful values that allow for the comparison of different orbits. The outputs are the ECI position and velocity, the spacecraft's RA and declination (DEC), the distance between the observatory and the spacecraft, and several angles which help determine whether observations can be made at the observatory at that point. These angles will be discussed more in depth in Sec. 4.1.

To test the accuracy of this numerical integration model, a Keplerian propagation of an elliptical orbit test case was run and compared to the model used. A plot of the position and velocity error between integration using Eq. (1) and Keplerian propagation over five orbits with a time

Downloaded From: https://www.spiedigitallibrary.org/journals/Journal-of-Astronomical-Telescopes,-Instruments,-and-Systems on 24 Jul 2023
Terms of Use: https://www.spiedigitallibrary.org/terms-of-use

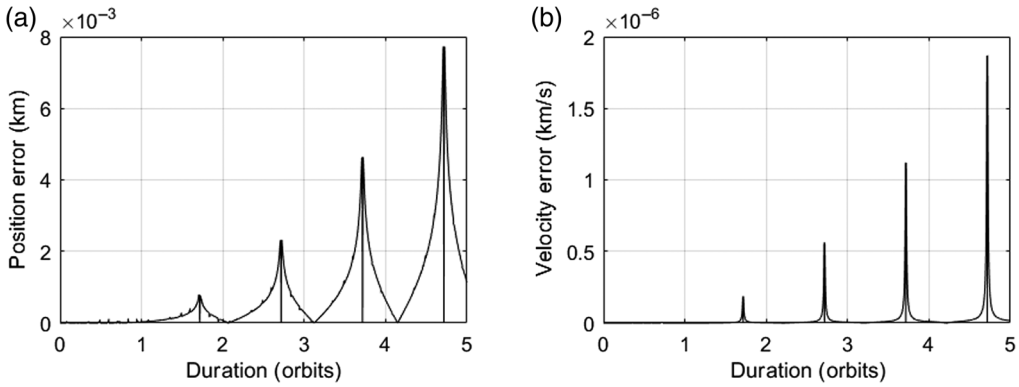

Fig. 2 Position and velocity error for an elliptical orbit between numerical integration model of Eq. (1) and standard Keplerian propagation over 5 orbits (25 days) with a time step of 1 s.

step of 1 s can be seen in Fig. 2. This plot shows error for a two-body system with no perturbations added, so the only error included is due to numerical integration. As shown, the position and velocity error stays below 8 m and 0.002 m/s, respectively, over a propagation interval of 25 days.

2.2 *Isoplanatic Frame*

In order to do useful science with an astrostationary orbit, two main conditions have to be met. First, the spacecraft has to be within some region of the sky known as the FOI, and second, it must stay within that region of sky for some specified length of time known as the time on target. In this section, a reference frame which can be used in the design of astrostationary orbits to determine whether these two conditions are met is defined.

Figure 3 shows the three main reference frames used in the design of astrostationary orbits. The blue frame is the standard ECI frame, where $\hat{\mathbf{Z}}_{\text{ECI}}$ is aligned with the Earth's spin axis and $\hat{\mathbf{X}}_{\text{ECI}}$ is aligned with the vernal equinox. The white frame is the Earth centered Earth fixed (ECEF) frame where $\hat{\mathbf{Z}}_{\phi} = \hat{\mathbf{Z}}_{\text{ECI}}$ and $\hat{\mathbf{Y}}_{\phi}$ is aligned with the longitude of the ground station. The dotted white line in this figure shows the vector from the center of the Earth to the ground station. Then the yellow dotted line shows the vector from the ground station to the target, which can be any region of the sky but here is depicted as a star.

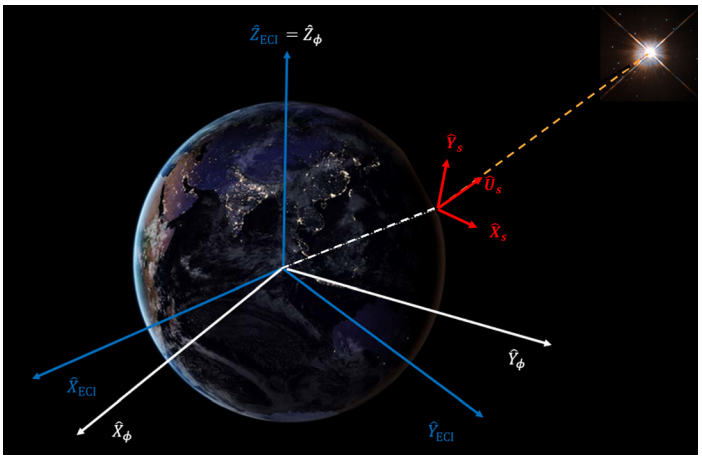

Fig. 3 The key reference frames used in the development of astrostationary orbits. These include the ECI frame (blue), the ECEF frame (white), and the isoplanatic frame (red).

Downloaded From: https://www.spiedigitallibrary.org/journals/Journal-of-Astronomical-Telescopes,-Instruments,-and-Systems on 24 Jul 2023
Terms of Use: https://www.spiedigitallibrary.org/terms-of-use

The isoplanatic frame (S), shown in red in this figure, is defined by the right-handed triad $[\hat{\mathbf{X}}_s, \hat{\mathbf{Y}}_s, \hat{\mathbf{U}}_s]$, where $\hat{\mathbf{U}}_s$ is a unit vector pointing from the ground station to an astronomical target. This is defined as

$$\hat{\mathbf{U}}_s = \begin{bmatrix} \cos\delta\cos\alpha \\ \cos\delta\sin\alpha \\ \sin\delta \end{bmatrix}, \tag{2}$$

where α and δ are the target's RA and declination, respectively. The vector $\hat{\mathbf{X}}_s$ is defined as

$$\hat{\mathbf{X}}_s = -(\hat{\mathbf{U}}_s \times \hat{\mathbf{Z}}_{\mathrm{ECI}}). \tag{3}$$

The relative position to the space component from the ground telescope in the ECI frame as a function of time t is defined as $d\vec{\mathbf{R}}_{\mathrm{ECI}}(t)$. The orbit component parallel [Eq. (4)] and perpendicular [Eq. (5)] to the unit direction of the star can be calculated using

$$d\vec{\mathbf{R}}_{||\mathrm{LOS}}(t) = \hat{\mathbf{U}}_s \cdot d\vec{\mathbf{R}}_{\mathrm{ECI}}(t), \tag{4}$$

$$d\vec{\mathbf{R}}_{\perp\mathrm{LOS}}(t) = d\vec{\mathbf{R}}_{\mathrm{ECI}}(t) - d\vec{\mathbf{R}}_{||\mathrm{LOS}}(t). \tag{5}$$

We are now able to obtain the position offset $\delta\vec{\mathbf{R}}_s(t)$ of the spacecraft from the line of sight vector $\hat{\mathbf{U}}_s$ as a function of time:

$$\delta\vec{\mathbf{R}}_s(t) = R_s^{\mathrm{ECI}} d\vec{\mathbf{R}}_{\perp\mathrm{LOS}}(t), \tag{6}$$

where R_s^{ECI} is the rotation matrix from the ECI frame to the isoplanatic frame. This equation can determine if and when the two astrostationary conditions are met. The space component will be within the FOI when

$$\|\delta\vec{\mathbf{R}}_s(t)\| < \|d\vec{\mathbf{R}}_{||\mathrm{LOS}}(t)\| \sin\beta_{\mathrm{FOI}}, \tag{7}$$

where β_{FOI} is the maximum angular distance from the line of sight $\hat{U}_s$ in which the FOI lies.

There are two conditions which determine if a given orbit has an astrostationary orbit related event. The first is that the spacecraft must be within an FOI dependent on the application and the ground station. Equation (7) can be used to determine whether this first condition is met. The second astrostationary condition is that the spacecraft must remain in that FOI for a given observation time. The length of time that Eq. (7) continues to hold will determine whether this condition has been met. If an orbit meets these two conditions at any point it can be defined as astrostationary.

3 Development and Initial Results for Two Example Astrostationary Orbits

As stated previously, there are many potential applications of hybrid ground and space observatories. This paper focuses on those that require astrostationary orbits, but there are many different orbit families that will meet astrostationary orbit conditions. Depending on the mission under consideration, different orbit families can be used to support different requirements and mission goals. For the sake of being concise, this paper presents only two of the candidate astrostationary orbit families. These are examples that work well for missions with a small FOI (< 15 arc sec radius) and a long required time in FOI (> 15 min). These include an HEO and a Sun/Earth L2 libration point orbit. Orbits are defined based on the astrostationary requirements described and an example propagated orbit is shown for each. Then initial results for each orbit family are presented and the two are compared.

Downloaded From: https://www.spiedigitallibrary.org/journals/Journal-of-Astronomical-Telescopes,-Instruments,-and-Systems on 24 Jul 2023
Terms of Use: https://www.spiedigitallibrary.org/terms-of-use

3.1 *Highly Elliptical Orbit*

The first orbit presented is an HEO which allows the spacecraft to inertially align with a ground observatory near apoapsis. At observation, the spacecraft must be on the line of sight from the observatory to the target, and the magnitude of its velocity component normal to the observatory line of sight must closely match that of the ground observatory to give as much time as possible on target. This orbit has been proposed previously[11–19] but has been enhanced here to include multiple potential observations during the orbit. This orbit is closer to Earth than the other orbit families, offering better communication and navigation. It also offers repeat observations after one period in case of low visibility.

Orbits have six degrees of freedom. Two position degrees of freedom are defined by the spacecraft being on the line of sight from the observatory to the target at the time of observation. Next, the distance at observation (d_{LOS}) can be defined by the user. This is the distance along the line of sight at observation and constrains the third position degree of freedom, and it can be freely defined within the range of distances given by the requirements. Larger separations will give longer observation times but also a longer time between observations due to a longer orbit period. At this point, the position is fully defined and the following equation can be written

$$\mathbf{r}_{\mathrm{ECI}}^{\mathrm{sc}} = \mathbf{r}_{\mathrm{ECI}}^{\mathrm{ob}} + d_{\mathrm{LOS}}\hat{\mathbf{U}}_{\mathbf{s}}. \tag{8}$$

Note that here, the superscript sc refers to the spacecraft and the superscript ob refers to the observatory. Similarly, two velocity degrees of freedom are defined by the fact that the velocity of the spacecraft perpendicular to the line of sight must match the velocity of the observatory perpendicular to the line of sight. The third degree of freedom is defined by the user selecting the period of the orbit. For the elliptical orbit, it is useful to choose an orbit period commensurable to the sidereal day and define the semimajor axis using

$$a = \left(\frac{\mu n^2 T_{\mathrm{sid}}^2}{4\pi^2}\right)^{\frac{1}{3}}. \tag{9}$$

Here n is the number of days in the period and T_{sid} is the length of the sidereal day. Note that the commensurability requirement can easily be relaxed to further optimize the orbit. The orbit period should be carefully selected by the user, because choosing an orbit period which is too short can result in an orbit which passes very close to Earth. In general, applications will have a minimum perigee requirement, and this should be taken into consideration when selecting the orbit period.

With these requirements, there is still one remaining binary degree of freedom. There are two orbits which meet the requirements with equal speed but opposite direction, so the user must determine whether the velocity will be positive (an input of 1) or negative (an input of -1).

Once the design is fully constrained, the orbit position and velocity can be calculated. The vis-viva equation is used to relate position ($\mathbf{r}_{\mathrm{ECI}}^{\mathrm{sc}}$), the semimajor axis ($a$), and velocity ($\mathbf{v}_{\mathrm{ECI}}^{\mathrm{sc}}$):

$$\|\mathbf{v}_{\mathrm{ECI}}^{\mathrm{sc}}\| = \sqrt{2\mu\left(\frac{1}{\|\mathbf{r}_{\mathrm{ECI}}^{\mathrm{sc}}\|} - \frac{1}{2a}\right)}. \tag{10}$$

As stated earlier, the spacecraft velocity perpendicular to the line of sight must be equal to the observatory velocity perpendicular to the line of sight, which can be expressed by

$$\mathbf{v}_{\mathrm{ECI},\perp}^{\mathrm{sc}} = \mathbf{v}_{\mathrm{ECI}}^{\mathrm{ob}} - (\mathbf{v}_{\mathrm{ECI}}^{\mathrm{ob}} \cdot \hat{\mathbf{U}}_s)\hat{\mathbf{U}}_s. \tag{11}$$

Based on this result, the velocity parallel to the line of sight can be calculated as

Downloaded From: https://www.spiedigitallibrary.org/journals/Journal-of-Astronomical-Telescopes,-Instruments,-and-Systems on 24 Jul 2023
Terms of Use: https://www.spiedigitallibrary.org/terms-of-use

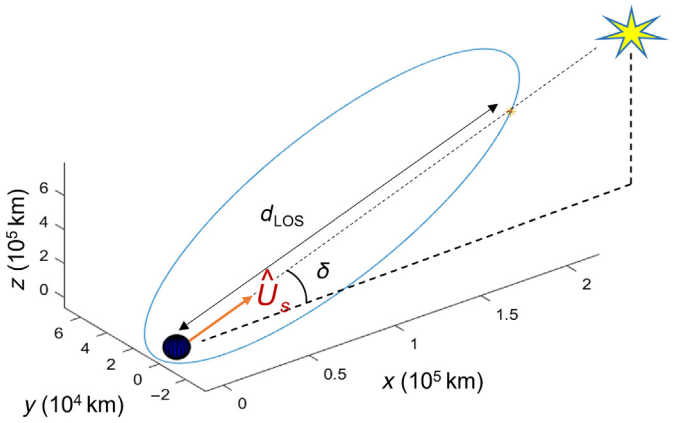

Fig. 4 Example HEO shown in ECI frame with inputs $\delta = 20$ deg, $\alpha = 0$ deg, $\phi = 19.826$ deg, $\lambda = 0$ deg, $d_{\text{LOS}} = 200{,}000$ km, and $n = 5$ days. The variables d_{LOS} and δ and the direction of $\hat{\mathbf{r}}$ are shown, α is zero so it cannot be seen.

$$\mathrm{v}^{\mathrm{sc}}_{\mathrm{ECI},\|} = \sqrt{\|\mathbf{v}^{\mathrm{sc}}_{\mathrm{ECI}}\|^2 - \|\mathbf{v}^{\mathrm{sc}}_{\mathrm{ECI},\perp}\|^2}. \tag{12}$$

The velocity of the spacecraft taken in the ECI frame is now fully defined. The chosen velocity direction determines the sign of the velocity expressed in the ECI frame parallel to the line of sight. The full definition of the velocity of the spacecraft is

$$\mathbf{v}^{\mathrm{sc}}_{\mathrm{ECI}} = \mathbf{v}^{\mathrm{sc}}_{\mathrm{ECI},\perp} \pm (\mathrm{v}^{\mathrm{sc}}_{\mathrm{ECI},\|})\hat{\mathbf{U}}_s. \tag{13}$$

With the full definition of the position and velocity, the HEO has been fully defined based on three user inputs: the distance along the line of sight, the period of the orbit, and the velocity direction (± 1).

Figure 4 shows an example elliptical orbit. The orbit is for a target at 20 deg declination and 0 deg RA and aligns with the W. M. Keck Observatory in Mauna Kea, HI. The user inputs given were a distance along the FOI of 200,000 km, a period of 5 days, and a velocity direction of $+1$. As shown, the astrostationary alignment will occur about 1 day prior to apoapsis.

3.2 *Libration Point Orbit*

In the synodic frame, the restricted three-body problem has five equilibrium points in which system forces balance due to the rotating frame. These points are known as Lagrange or libration points. Their approximate location can be seen in Fig. 5. As the system rotates over time, the Lagrange points rotate with it.

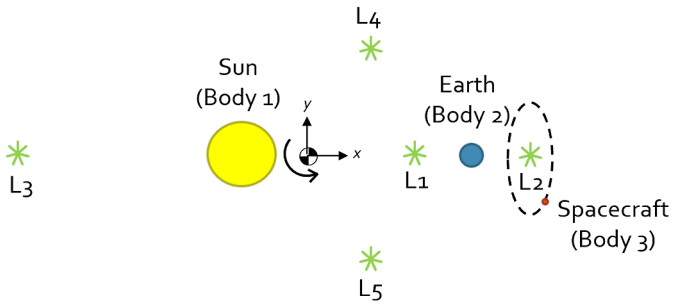

Fig. 5 Lagrange point locations in the restricted three-body problem for the Earth–Sun system, with an example halo orbit at the L2 point to show the location of the spacecraft.

Downloaded From: https://www.spiedigitallibrary.org/journals/Journal-of-Astronomical-Telescopes,-Instruments,-and-Systems on 24 Jul 2023
Terms of Use: https://www.spiedigitallibrary.org/terms-of-use

Halo orbits can form around Lagrange points 1, 2, and 3 in Fig. 5. In the Sun/Earth system, both points 1 and 2 have potential applications for astrostationary orbits. In either, the spacecraft would be moving slowly enough with respect to a ground station that astrostationary alignment opportunities would occur every night. An L2 orbit would be useful for night sky astronomical observations, whereas an L1 orbit would be useful for heliophysics observations. Another promising set of orbits would be around either the L2 or L3 point in the Earth/Moon system, which would have a higher velocity that the Sun/Earth orbits but could still allow for near-astrostationary alignments. The method presented in this section goes through the development of an orbit around the L2 point in the Sun/Earth system, but this approach is general and can be applied to other cases.

Libration point orbits offer longer observation times, but the spacecraft would be about 1.5 million km from Earth in a Sun/Earth L1 or L2 point orbit, making communication and navigation more difficult. However, it would also have significantly lower fuel costs for reconfiguration than the HEO, both because of its distance from Earth and its ability to move across the observable sky and view many targets in a single orbit. In this section, the development of a libration point orbit in the Sun/Earth system around the L2 point is presented.[21,22] The orbit is calculated using normalized values. First, the value μ is calculated using

$$\mu = \frac{\mu_2}{\mu_2 + \mu_1}. \tag{14}$$

Here μ_2 is the gravitational parameter for the smaller body, and μ_1 is the gravitational parameter for the larger body. A new reference frame known as the rotating libration point (RLP) frame is defined to describe the halo orbit. In this normalized frame, the origin is at the L2 point, the **x** vector points away from the larger body, the **z** vector is defined by the angular momentum of the synodic frame, and the **yy** vector completes the right-handed triad. The equations to move into the RLP frame from the synodic frame are given as follows:

$$\bar{x} = \frac{x/d_{\mathrm{EL}} - 1 + \mu \pm \gamma}{\gamma}, \tag{15}$$

$$\bar{y} = \frac{y/d_{\mathrm{EL}}}{\gamma}, \tag{16}$$

$$\bar{z} = \frac{z/d_{\mathrm{EL}}}{\gamma}, \tag{17}$$

where d_{EL} is the distance between Earth and the libration point, and γ is defined as the unique solution to

$$\gamma^5 \mp (3-\mu)\gamma^4 + (3-2\mu)\gamma^3 - \mu\gamma^2 \pm 2\mu\gamma - \mu = 0, \tag{18}$$

where the upper sign is for an L1 orbit and the lower sign is for an L2 orbit.[22] The system has now been scaled so that the distance between the libration point of interest and the Earth is 1. This system enables the use of simple equations of motion which can be used to propagate the libration point orbit.

The orbit is initialized at the point in the orbit where $y, \dot{x}$, and $\dot{z}$ are all zero, which is done to immediately define three degrees of freedom and make the process of defining the remaining position and velocity variables based on the observatory and target star locations more straightforward. However, it should be noted that observations can be made at any point in the libration point halo orbit. The values of y, $\dot{x}$, and $\dot{z}$ are all zero at both the points indicated by red dots in Fig. 6. The values x and $\dot{y}$ are related by a constant in order to make the orbit periodic. Since libration points 1 to 3 are unstable equilibrium points, only one y velocity will result in a stable halo orbit for a given x position, otherwise, the orbit will not be stable and will move away from the L2 point.[22] This constrains a fourth degree of freedom. Next, the initial z value of the halo orbit is defined based on the target star declination, and the y velocity is set equal to the observatory velocity perpendicular to the line of sight. The orbit is now fully constrained.

Downloaded From: https://www.spiedigitallibrary.org/journals/Journal-of-Astronomical-Telescopes,-Instruments,-and-Systems on 24 Jul 2023
Terms of Use: https://www.spiedigitallibrary.org/terms-of-use

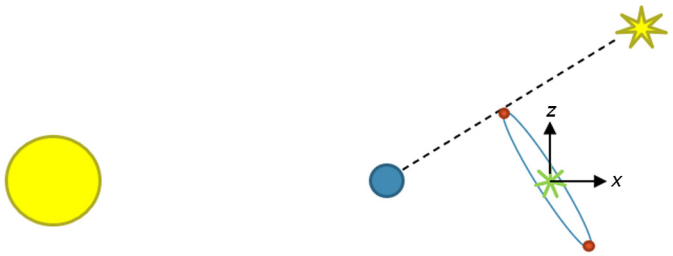

Fig. 6 L2 point halo orbit. The axes show the normalized RLP frame, and the red dots denote the points at which y_{RLP}, $\dot{x}_{RLP}$, and $\dot{z}_{RLP}$ are all zero.

Libration point orbits are very sensitive to initial conditions and numerical propagation steps. These initial conditions could be used with the model described but the step size would have to be very small, so a state transition matrix was used to propagate the example orbits in this paper. The state transition matrix has previously been defined[21,22] and is defined as

$$A = \begin{bmatrix} 0 & 0 & 0 & 1 & 0 & 0 \\ 0 & 0 & 0 & 0 & 1 & 0 \\ 0 & 0 & 0 & 0 & 0 & 1 \\ 1+2c_2 & 0 & 0 & 0 & 2 & 0 \\ 0 & 1-c_2 & 0 & -2 & 0 & 0 \\ 0 & 0 & -c_2 & 0 & 0 & 0 \end{bmatrix}. \tag{19}$$

Here c_2 is the constant defined by

$$c_n = \frac{1}{\gamma^3}\frac{((-1)^{L+1})^n\mu + (-1)^n(1-\mu)\gamma^{n+1}}{(1+(-1)^{L\gamma})^{n+1}}, \tag{20}$$

where n is a constant, in this case 2, and L is the Lagrange point the halo orbit is being propagated around. At each time t, the state of the orbit is

$$\bar{X} = e^{At}. \tag{21}$$

An example orbit formed in the Sun/Earth system at the L2 point can be seen in Fig. 7(a). The orbit is designed for a declination of 20 deg and an RA of $\alpha = 0$ deg with the W. M. Keck Observatory.

This orbit was then converted to the ECI frame in Fig. 7(b) and (c). Note that the L2 point appears as a point in the rotating synodic frame but in the inertial ECI frame it will orbit the

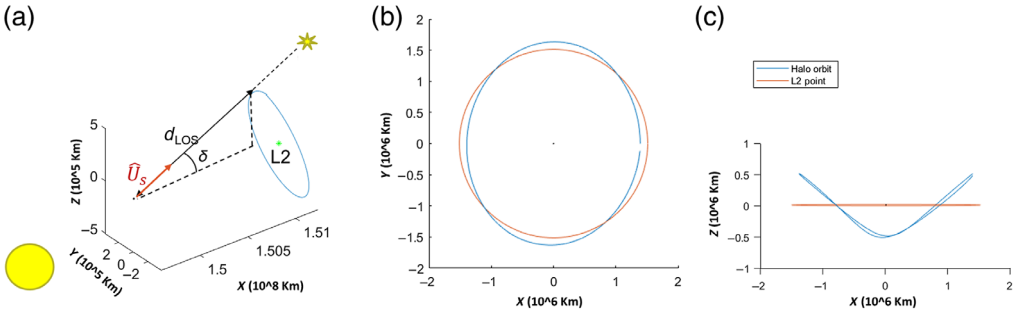

Fig. 7 (a) Example L2 point halo orbit shown in the Sun–Earth synodic frame with inputs $\delta = 20$ deg, $\alpha = 0$ deg, $\phi = 19.826$ deg, and $\lambda = 0$ deg. The variables d_{LOS} and δ and the direction of $\hat{\mathbf{U}}_s$ are shown. (b), (c) Same L2 point halo orbit shown in ECI frame. The L2 point in the ECI frame over time is shown in red, and the spacecraft's path is shown in blue. The ECI xy plane is shown in (b) and the ECI xz plane is shown in (c).

Downloaded From: https://www.spiedigitallibrary.org/journals/Journal-of-Astronomical-Telescopes,-Instruments,-and-Systems on 24 Jul 2023
Terms of Use: https://www.spiedigitallibrary.org/terms-of-use

Earth. The halo orbit is orbiting the L2 point, so it moves around the Earth while also changing its position relative to the L2 point.

3.3 *Initial Results*

In this section, initial results for the two example orbit families developed are presented. First, the path in the FOI for a given target in Fig. 8 is shown. Results are given for two different target declinations for both of the orbit families. As shown, a change in declination can result in a large difference in the shape of the path through the FOI. Note that these paths are not fully optimized for time in the FOI, and so the amount of time for both can be increased. This process is discussed further in Sec. 4.

As shown, the path in the FOI for both orbit families is quite similar. However, the time in the FOI is where the orbit families start to significantly differ. The time in the FOI is highly dependent on the target declination and the FOI radius. Figure 9 shows the time in FOI for a range of declinations for both orbit families. Note that RA does not effect the time in FOI as long as the spacecraft is on the telescope meridian when on target. The FOI radius for all results in this figure is 7.3 arc sec.

As shown, the libration point orbits have significantly longer times in the FOI than the elliptical orbit family. All the orbits give times longer than about 30 min, but the libration point orbits can have times as long as 3.5 h. This is due to the fact that the velocity of the orbit is not changing as quickly with respect to the ground station as that of the elliptical orbit.

The next result is the observable sky. The path of the spacecraft on the elliptical orbit can be seen in Fig. 10(a). In addition to showing the spacecraft path, this plot also shows the observable regions. These are defined based on two common ground observatory requirements: first, that the angle between the zenith and the pointing vector to the Sun is ≥ 110 deg and second, that the angle between the zenith and the pointing vector to the spacecraft is < 60 deg. Sections of the orbit that meet both those requirements are highlighted in black. Note that all five regions

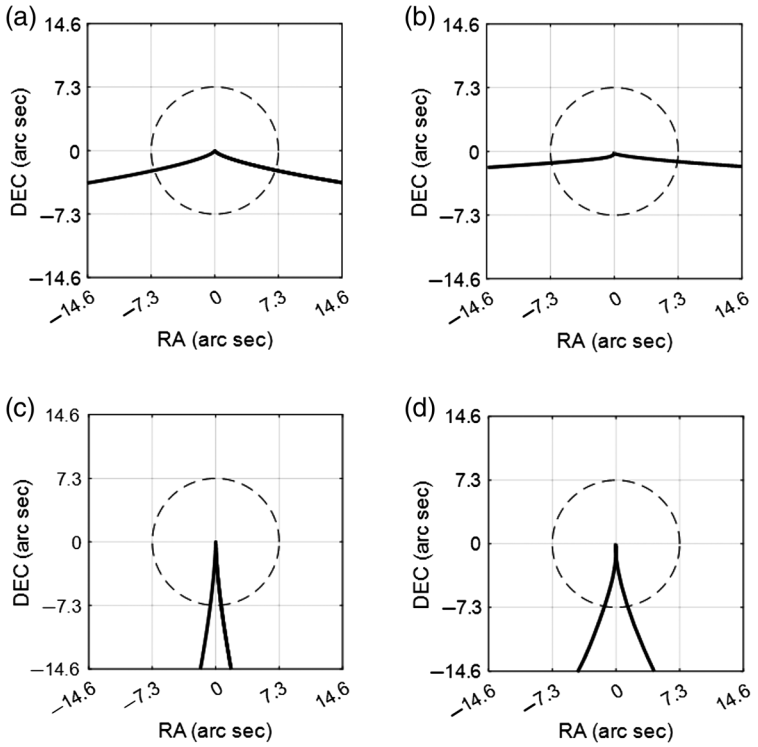

Fig. 8 Path of spacecraft through FOI (7.3 arc sec) for (a) an elliptical orbit with a target declination of 1 deg; (b) a halo orbit with a target declination of 1 deg; (c) an elliptical orbit with a target declination of 20 deg; and (d) a halo orbit with a target declination of 20 deg.

Downloaded From: https://www.spiedigitallibrary.org/journals/Journal-of-Astronomical-Telescopes,-Instruments,-and-Systems on 24 Jul 2023
Terms of Use: https://www.spiedigitallibrary.org/terms-of-use

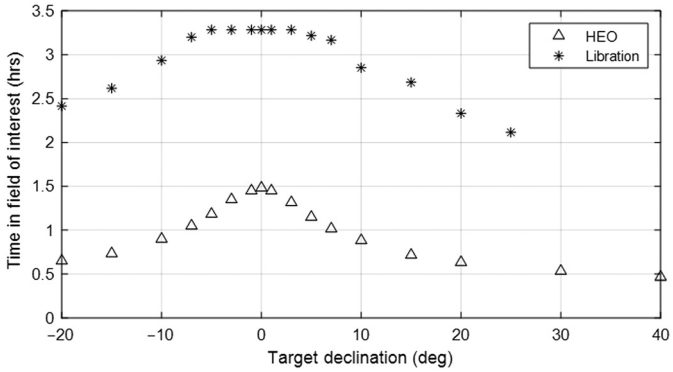

Fig. 9 Time in FOI for the elliptical and libration point orbit families over a range of target declinations. All results are given for a 7.3-arc sec radius FOI.

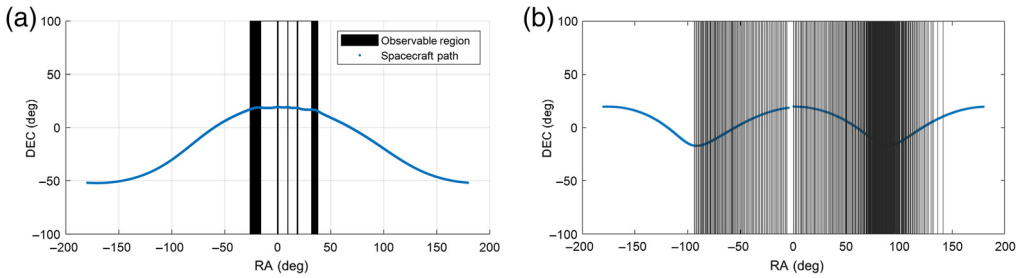

Fig. 10 The observable sky for (a) an example elliptical orbit (4.5 day orbit period) and (b) libration point orbit (1 year) with a target declination of 20 deg and RA of 0 deg over one orbit period. The observable regions show areas where the angle between the zenith and the pointing vector to the Sun is >110 deg and the angle between the zenith and the line of sight vector is < 60 deg. For the libration point orbit, we assume that the orbit is maintained throughout the year. Observations cannot be made for about 1/3 of the year because the observation time would be during the day.

last the same amount of time, but for the two thicker regions the spacecraft is moving faster so covers a broader section of the sky.

The same plot can be seen for the libration point orbit in Fig. 10(b). As shown, these orbits take one year in the ECI frame, so there are many more observation opportunities. The observation opportunities occur about once per day for about two thirds of the year. Note that this plot assumes that the orbit will remain in the halo orbit for the entire year, which will require small maneuvers to keep the spacecraft in the orbit. This offers a much larger range of the observable sky without using any fuel for reconfiguration. The libration point orbit would also have comparatively low reconfiguration costs compared to the HEO case, and so the number of observations that could be made for the amount of fuel used would be signficantly higher for the libration point orbit than for the elliptical orbit.

The final result is the change in RA and declination over time. Figure 11(a) shows the change in RA over a single elliptical orbit, with Earth's J2, Sun, and Moon perturbations included. The gray regions show the sections when the observability requirements are met. As shown, there are three locations where the change in RA and declination are both <0.1 arc sec /s at the same time, representing three potential regions where the orbit has the potential to be astrostationary. There is no requirement on the change in RA and declination, but this plot helps show the regions where the spacecraft will be moving slowly enough to stay in an FOI for a significant period of time.

Similar results for the libration point orbit can be seen in bottom plot. The orbit was propagated for the first 10 days, which is representative of the full year. As shown, the change in RA and declination (DEC) for the orbit is significantly lower than for the elliptical orbit. This presents longer observation opportunities and allows for an observation every night.

Downloaded From: https://www.spiedigitallibrary.org/journals/Journal-of-Astronomical-Telescopes,-Instruments,-and-Systems on 24 Jul 2023
Terms of Use: https://www.spiedigitallibrary.org/terms-of-use

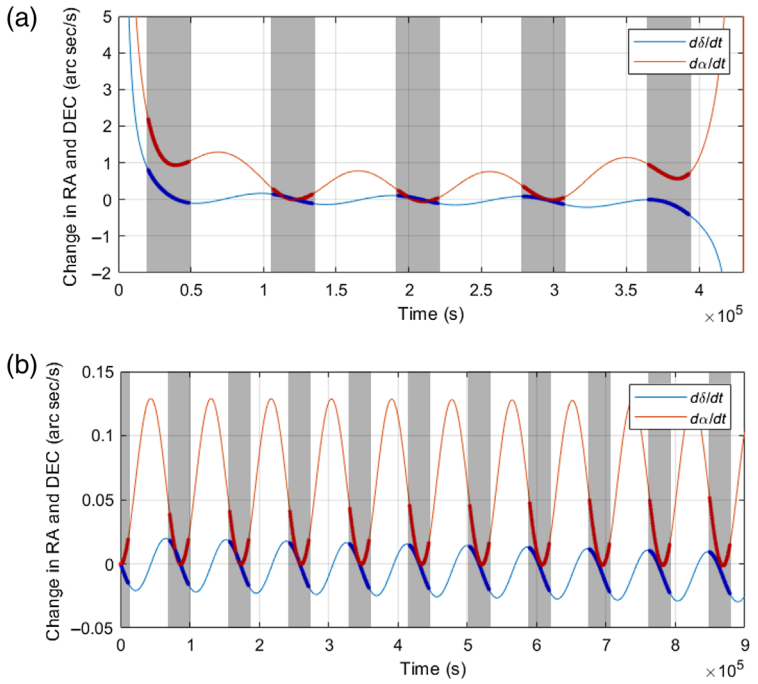

Fig. 11 The change in spacecraft RA and declination (DEC) for (a) an example elliptical orbit and (b) libration point orbit with a target declination of 20 deg and RA of 0 deg. The observable regions shown in gray are areas where the angle between the zenith and the pointing vector to the Sun is >110 deg and the angle between the zenith and the line of sight vector is <60 deg. The elliptical orbit is shown over one 5-day period and libration point orbit is shown for the first 10 days of the orbit. Note that the first 10 days are representative of the full year.

4 Example Mission: ORCAS

ORCAS is a proposed mission which would use a hybrid space and ground observatory to allow ground telescopes to greatly increase their angular resolution, sensitivity, and science target accessibility using a laser guide star to improve AO. The laser guide star would be on a SmallSat spacecraft and would need to align with a ground observatory and an astronomical observation target.

In this section, the ORCAS mission and its requirements are described. ORCAS is used as an example application of astrostationary orbits. An orbit family which will meet the mission requirements is selected and developed further to enhance its performance. ORCAS should provide an example as to the design of orbits for applications where a ground station and a space component are working together.

4.1 *Mission Requirements*

There are several requirements for ORCAS that must be taken into consideration when designing an orbit for the mission. These are listed below. Figures describing these angle requirements have previously been discussed in detail.[2,23]

1. The telescope shall be pointed within 60 deg of the local zenith angle.

   As the angle between the telescope pointing vector and the local zenith angle (θ) increases, the amount of atmospheric distortion increases.
2. The angle between the local zenith and the pointing vector to the Sun shall be >110 deg.

   The limit on the angle between the local zenith direction and the pointing vector to the Sun (ψ) ensures that it is night at the observatory when observations are taken. This corresponds to an approximate local solar time of 7:30 pm to 4:30 am.
3. The normal vector to the spacecraft face plane shall be within 89 deg to the Sun.

   This ensures that sunlight does not directly illuminate the face of the spacecraft pointed at the ground based telescope, which would interfere with the laser signal.

Downloaded From: https://www.spiedigitallibrary.org/journals/Journal-of-Astronomical-Telescopes,-Instruments,-and-Systems on 24 Jul 2023
Terms of Use: https://www.spiedigitallibrary.org/terms-of-use

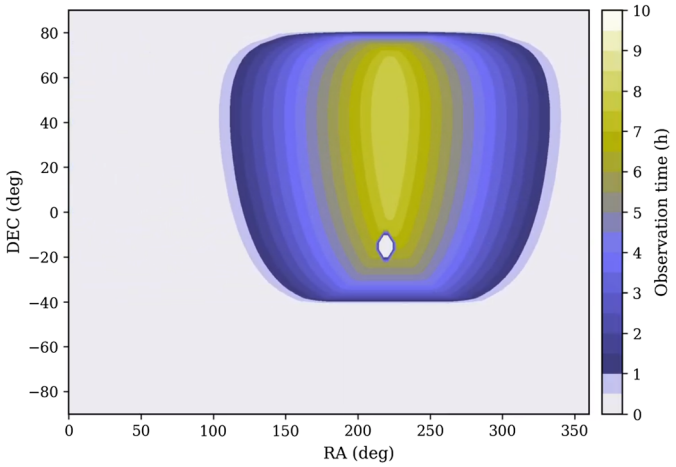

Fig. 12 The observable sky for ORCAS working with W. M. Keck Observatory on a night in June 2025, contoured according to available observation time for each possible celestial coordinate. Each location in this map requires a different orbit choice to achieve the astrostationary condition.

4. The normal vector to the spacecraft shall be within 80 deg from the line of sight.
   This angle is required to maintain proper communication with the ground.
5. The spacecraft perigee altitude shall be at least 1000 km.
   The perigee requirement is based on safety. At 1000 km, collisions with spacecraft and debris in low Earth orbit are less likely and the spacecraft woould not reenter the atmosphere if there are any problems with the propulsion system.
6. The spacecraft shall remain within the telescope's FOI along the line of sight from the observatory to the target star for a user-specified minimum time.

The range in time is based on the application. For example, if an astonomical observation were being done, imaging a supernova takes 10 min, whereas imaging an exoplanet takes up to 2 h.[24] The estimated range for a length of time that would allow for useful applications is 10 min to 3 h. This range is given as a guideline; however, observations >3 h are acceptable and welcome.

Taking these requirements into account results in a map of the observable sky for any given date. An example observable sky map can be seen in Fig. 12. The contoured region corresponds to the integrated area under a spherical sector rotating around the Earth at night with a region of forbidden spacecraft positions removed. More details on making this figure have been previously described.[23]

All of these requirements could be met by both astrostationary orbits presented in Sec. 3. The HEO was chosen for ORCAS for several reasons. Both the libration point and HEOs would have worked, but the HEO is much closer to Earth, so the design of the spacecraft is simpler. The navigation and communication systems can be high technology readiness level systems, giving the HEO an edge. However, the libration point orbit would give longer observation times and lower costs for reconfiguring the orbit, so it should be considered for future missions with similar requirements to those of ORCAS.

4.2 *Further Development of HEO*

In this section, further development of the HEO family chosen for ORCAS is presented. Three observation opportunities which are available for this orbit are discussed and results on tuning the orbit to have a significantly longer time in the FOI are presented.

4.2.1 *Three observations per orbit*

The development of the HEO is based on the observation of one target star. Because the orbit is designed for that particular star, the longest observation time in the orbit will take place there.

Downloaded From: https://www.spiedigitallibrary.org/journals/Journal-of-Astronomical-Telescopes,-Instruments,-and-Systems on 24 Jul 2023
Terms of Use: https://www.spiedigitallibrary.org/terms-of-use

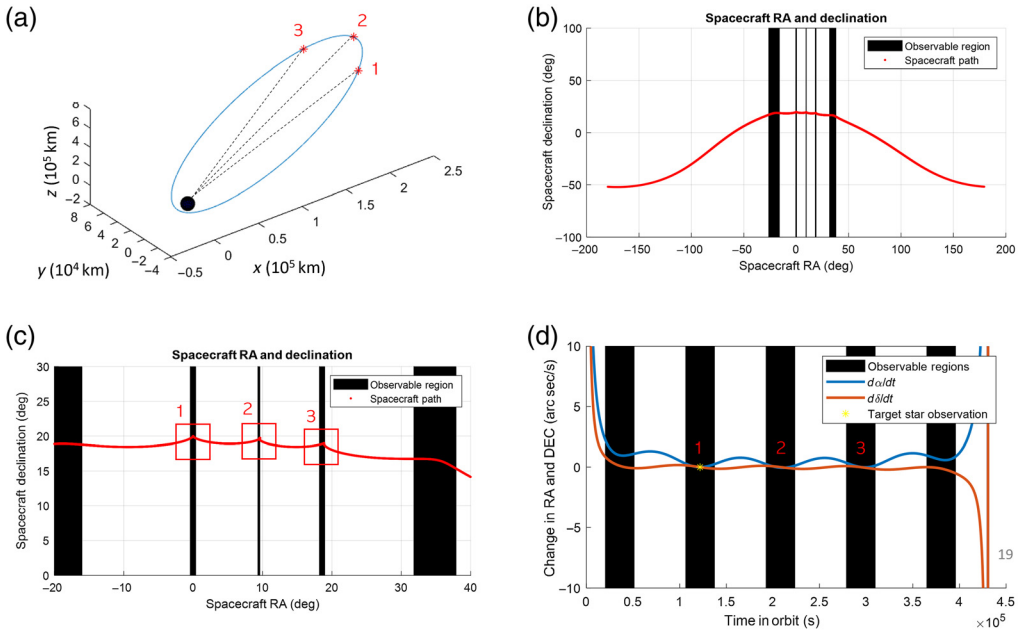

Fig. 13 (a) Example orbit in ECI frame with a target star declination of 20 deg with dotted lines showing the line of sight to the locations in the orbit where AO observations can be made. (b) ORCAS spacecraft RA and declination over one orbit with observable regions where observation angle requirements are met in black. (c) ORCAS spacecraft RA and DEC showing the three AO observation points. (d) The change in RA and declination of the spacecraft over one orbit period with observable regions shown in black and the three AO observation points labeled.

However, there are two other points in the orbit where the spacecraft is moving slowly enough that the time on target is significant and useful science can be done. Figure 13 shows the location of these three observation points for an example elliptical orbit with a target observation declination of 20 deg and how they were discovered. Figure 13(a) shows the elliptical orbit and the three opportunities. Figure 13(b) shows the spacecraft's path across the sky, and Fig. 13(c) shows a more zoomed in version of that plot, in which three peaks are shown. These are places where the spacecraft remains nearly stationary in the sky for a long period of time. Finally, Fig. 13(d) shows the change in RA and declination throughout the orbit. As seen in that plot, there are three locations where the change in both values is <0.1 arc sec /s at the same time.

Figure 14 shows each of the observations in an FOI of 0.3×0.3 deg and then at 7.3×7.3 arc sec. In this figure, the results are all for an example elliptical orbit with a target declination of 20 deg for the first observation. All three have an FOI radius of 7.3 arc sec. The first observation will have a time on target of 52 min. The second observation will be on target for 8 min, and the third observation will have a time on target of 35 min. Based on these observation times, any of these three observations could be used for AO imaging.

As shown, the second observation opportunity occurs at apogee, where the overall velocity of the spacecraft is lowest. The overall velocity is very slow but some of that velocity is still perpendicular to the line of sight vector, so this offers an observation opportunity of several minutes. The third opportunity occurs at the point in the orbit where the spacecraft is equally far from apogeee as the first observation but on the other side. As shown, this observation has a more similar shape to the first observation. The spacecraft velocity perpendicular to the line of sight is much closer to zero than at apogee. This allows for a time on target of about 60% of the time available from the first observation.

In addition to AO observations, the ORCAS spacecraft could also be used for flux calibration. Flux calibration only requires a laser streaking across the FOI, so whenever AO observations are not taking place and the spacecraft is in the observable sky for the ground station, flux calibration observations can take place. It should be noted here that choosing the Lagrange halo orbit instead of the HEO would offer more potential in terms of the number of stars which can be

Downloaded From: https://www.spiedigitallibrary.org/journals/Journal-of-Astronomical-Telescopes,-Instruments,-and-Systems on 24 Jul 2023
Terms of Use: https://www.spiedigitallibrary.org/terms-of-use

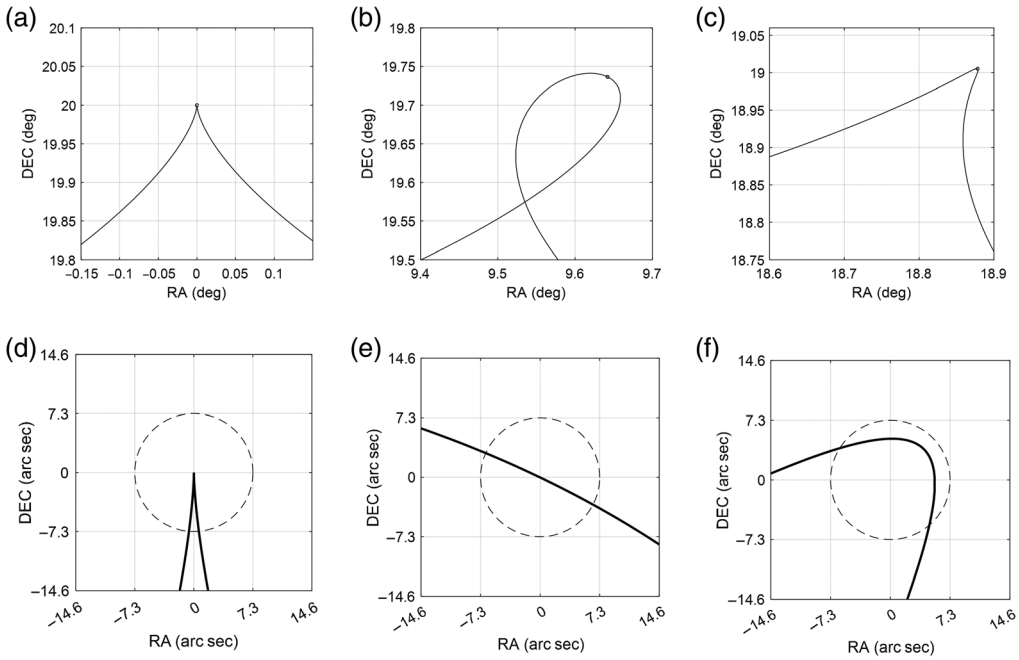

Fig. 14 The three observation opportunities for an HEO. Results are shown for a target at 20 deg declination and 0 deg RA. (a)–(c) The spacecraft path through a 0.3×0.3 deg patch of sky, with a black circle representing the FOI. (d)–(f) the FOI, which is assumed to be 7.3 arc sec. (a), (d) The first observation opportunity, which the orbit is designed for. The time on target is about 52 min. (b), (e) The second observation, which occurs at apogee. The time on target is about 8 min. (c), (f) The third observation opportunity, which has a time on target of about 35 min.

viewed using a single orbit, significantly reducing the fuel costs and potentially increasing the total number of observations.

4.2.2 *Increasing observation times*

The time on target for the HEO can be increased by further tuning the orbit. In the original development of the orbit, the HEO is designed to have a velocity perpendicular to the ground station which exactly matches the ground station. Additionally, the position is designed to

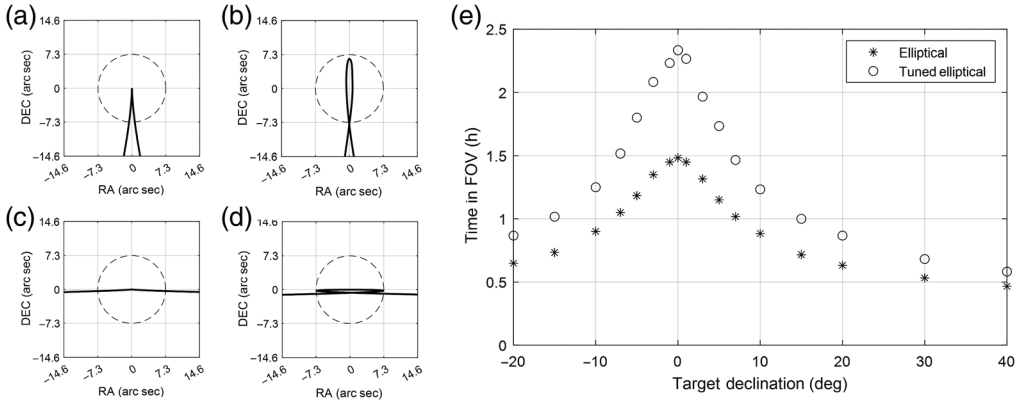

Fig. 15 (a) The untuned trajectory for the HEO designed for a target declination of 20 deg. (b) The tuned trajectory for the HEO designed for a target declination of 20 deg. (c) The untuned trajectory for the HEO designed for a target declination of 0 deg. (d) The tuned trajectory for the HEO designed for a target declination of 0 deg. (e) The time on target for the tuned and untuned elliptical orbit family at a range of target declinations. Results are for an FOI radius of 7.3 arc sec.

Downloaded From: https://www.spiedigitallibrary.org/journals/Journal-of-Astronomical-Telescopes,-Instruments,-and-Systems on 24 Jul 2023
Terms of Use: https://www.spiedigitallibrary.org/terms-of-use

exactly match the target star's position. However, the orbit can be further optimized to significantly increase the time on target. First, if the velocity of the spacecraft at observation perpendicular to the line of sight is slightly lower than that of the ground observatory, the trajectory in the line of sight will become a loop rather than the peak seen previously, as can be seen in Fig. 15. Additionally, if the position of the observation point is moved up within the FOI this can also add time in the FOI. An example of this for two HEOs designed for 20 deg and 0 deg declination, along with the times on target for both, can be seen in Fig. 15.

As shown, tuning the elliptical orbit can result in a significant increase in time on target for all declinations. At low declinations, the elliptical orbit can have a time on target of almost 2.5 h for an FOI radius of 7.3 arc sec.

5 Summary

We have presented a method which allows users to input an orbit and test whether it can meet astrostationary conditions. The model developed gives results on the orbit trajectory in the ECI frame, the isoplanatic frame defined in this paper, and the RA and declination frame. This allows users to determine how and where astrostationary conditions can be met by any given orbit.

In addition to developing this method, two example orbit families are presented which can be astrostationary. The development of an HEO and an L2 libration point orbit is discussed. For each of these orbits, initial results are given which show how they meet the astrostationary orbit conditions at multiple points throughout the orbit. Key results are presented for comparison, including the time on target, the trajectory through the FOI, and the change in RA and declination throughout the orbit. It is worth noting that future studies could include trades that take into account launch delta-v costs and maneuvering for an entire observation program to establish the most suitable orbit choice from a whole mission perspective.

Finally, an example of a hybrid space and ground observatory mission, ORCAS, is presented. The HEO family is selected, which is able to meet all requirements, and that orbit is further developed to provide the mission with three observation opportunities and a longer time on target. A concept for using the spacecraft to do flux calibration is also introduced. All of these results represent a significant increase in the science yield of the ORCAS mission.

The work presented in this paper forms a foundation for astrostationary orbits. Previous work in the field has primarily focused on using HEOs to meet the astrostationary conditions, whereas this work shows that in reality there are many different orbits which can be used for these types of applications. In addition to the two astrostationary orbits presented in this paper, these include orbits at the L1 point for solar observations, high inclination orbits near the L2 point distance, radial orbits for repeat observations of a special target, resonant Earth–Moon orbits, lower orbits for observations of Earth satellites in geosynchronous or geostationary orbits, orbits that align with the Hubble observatory, and orbits that align with L2 telescopes like the James Webb Space Telescope, Habitable Exoplanet Observatory, or Large UV/Optical/IR Surveyor. These additional orbits point to new applications including helio-stationary orbits which align with the Sun, geostationary orbits which would orbit the Earth once per day, orbits which align with space telescopes, and other cases for moving, accelerating, and rotating solar system objects. These additional orbit cases are described in more detail below.

References

1. P. Kurczynski, "Event horizon explorer mission concept step-1 proposal," FY22 IRAD Step-1 Proposal, eventhorizontelescope.org (2022).
2. A. W. Koenig et al., "Optimal spacecraft orbit design for inertial alignment with ground telescope," in *IEEE Aerosp. Conf.* (2021).
3. E. Peretz et al., "Exoplanet imaging scheduling optimization for an orbiting starshade working with extremely large telescopes," *J. Astron. Telesc. Instrum. Syst.* **7**(2), 021213 (2021).
4. E. Peretz et al., "Orbiting Configurable Artificial Star (ORCAS) for visible adaptive optics from the ground," *Bull. Am. Astron. Soc.* **51**(7), 284 (2019).

Downloaded From: https://www.spiedigitallibrary.org/journals/Journal-of-Astronomical-Telescopes,-Instruments,-and-Systems on 24 Jul 2023
Terms of Use: https://www.spiedigitallibrary.org/terms-of-use

5. E. Peretz et al., "Orbiting configurable artificial star multi-wavelength laser payload," *Proc. SPIE* **11820**, 118200F (2021).
6. E. Peretz et al., "ORCAS – orbiting configurable artificial star mission architecture," *Proc. SPIE* **11819**, 1181905 (2021).
7. P. L. Wizinowich et al., "The W. M. Keck Observatory laser guide star adaptive optics system: overview," *Publ. Astron. Soc. Pac.* **118**, 297–309 (2006).
8. D. M. Boroson et al., "The lunar laser communications demonstration (LLCD)," in *IEEE Int. Conf. Space Mission Challenges for Inf. Technol.* (2009).
9. D. J. Israel, B. L. Edwards, and J. W. Staren, "Laser communications relay demonstration (LCRD) update and the path towards optical relay operations," in *IEEE Aerosp. Conf.* (2017).
10. D. Rabin, "Orbiting artificial star for high-resolution coronal imaging from the ground," FY22 IRAD Step-2 Proposal (2022).
11. J. Albert, "Satellite-mounted light sources as photometric calibration standards for ground-based telescopes," *Astron. J.* **143**, 8 (2012).
12. J. Bailey, "Orbiting laser beacons for adaptive optics observations of Mars and other planets," *Publ. Astron. Soc. Pac.* **116**, 745–749 (2004).
13. G. D. Rico et al., "Ground-based adaptive optics observations with orbiting nanosatellite (GO-ON)," *Proc. SPIE* **11448**, 1144874 (2020).
14. R. Foy and A. Labeyrie, "Feasibility of adaptive telescope with laser probe," *Astron. Astrophys.* **152**, L29–L31 (1985).
15. A. Greenaway, "Satellite-borne laser for adaptive optics reference," *Proc. SPIE* **1494** (1991).
16. A. Greenaway and S. Clark, "PHAROS: an agile satellite-borne laser guide star," *Proc. SPIE* **2120**, 1–5 (1994).
17. W. A. Marlow et al., "Laser-guide-star satellite for ground-based adaptive optics imaging for geosynchronous satellites," *J. Spacecr. Rockets* **54**(3) (2017).
18. M. Noyes and M. Hart, "Analyzing the viability of satellite laser guide stars for breakthrough starshot," in *6th Int. Conf. Adapt. Opt. for Extremely Large Telesc.*, p. AO4ELT (2019).
19. W. Thompson and C. Marois, "Extremely bright orbital guide beacons for extremely large telescopes," in *6th Int. Conf. Adapt. Opt. for Extremely Large Telesc.*, p. AO4ELT (2019).
20. J. Albert and W. Burgett, "Telescope spectrophotometric and absolute flux calibration, and national security applications, using a tunable laser on a satellite," (2006).
21. K. C. Howell, "Three-dimensional, periodic, "halo" orbits," *Celest. Mech.* **32**(1), 53–71 (1984).
22. W. S. Koon et al., *Dynamical Systems, the Three-Body Problem and Space Mission Design* (conference paper), SourceOAI (2000).
23. E. Peretz et al., "Mapping the observable sky for a remote occulter working with ground-based telescopes," *J. Astron. Telesc. Instrum. Syst.* **7**(1), 021212 (2021).
24. E. Peretz et al., "Exoplanet imaging performance of envelopes for starshade-based missions," *J. Astron. Telesc. Instrum. Syst.* **7**(2), 021215 (2021).

Biographies of the authors are not available.

Downloaded From: https://www.spiedigitallibrary.org/journals/Journal-of-Astronomical-Telescopes,-Instruments,-and-Systems on 24 Jul 2023
Terms of Use: https://www.spiedigitallibrary.org/terms-of-use